Engineering Lithium Ion Battery Cathodes for High Voltage Applications Using Electromagnetic Excitation

Laisuo Su,[1] Shikhar Krishn Jha,[1] Xin Li Phuah,[2] Jiang Xu,[3] Nathan Nakamura,[1] Haiyan Wang,[2] John S. Okasinski,[4] and B. Reeja-Jayan[1, z]

[1] Department of Mechanical Engineering, Carnegie Mellon University, Pittsburgh, Pennsylvania, USA
[2] School of Materials Engineering, Purdue University, West Lafayette, Indiana, USA
[3] Civil and Environmental Engineering, Carnegie Mellon University, Pittsburgh, Pennsylvania, USA
[4] Advanced Photo Source, Argonne National Laboratory, Illinois, USA
[z] bjayan@andrew.cmu.edu

Abstract: Microwave radiation (MWR), a type of electromagnetic excitation source, reduces the synthesis temperature and processing time for chemical reactions compared to traditional synthesis methods. Recently, we demonstrated that MWR can engineer ceramics with different crystal phases compared to traditional methods [*Journal of Materials Chemistry A* **5**, 35 (2017)]. In this study, we further apply the MWR-assisted technique to improve the electrochemical performance of $LiCoO_2$ cathodes by engineering TiO_2 and ZrO_2 ceramic coatings. Electrochemical tests suggest that the TiO_2 coating improves the rate capability of the $LiCoO_2$ electrode. Both TiO_2 and ZrO_2 coatings improve the high voltage (4.5 V) cycling stability of $LiCoO_2$. The capacity remaining is improved from 52.8% to 84.4% and 81.9% by the TiO_2 coating and the ZrO_2 coating, respectively, after 40 cycles. We compare these results with existing studies that apply traditional methods to engineer TiO_2/ZrO_2 on $LiCoO_2$, and find that the MWR-assisted method shows better performance improvement. X-ray photoelectron spectroscopy measurements suggest that the improved cycling stability arises from the formation of metal fluorides that protect the electrode from side reactions with electrolytes. This mechanism is further supported by the reduced Co dissolution from TiO_2/ZrO_2 coated $LiCoO_2$ electrode after cycling. This study provides a new toolbox facilitating the integration of many delicate, low melting point materials like polymers into battery electrodes.

Keywords: Microwave radiation; Surface engineering; $LiCoO_2$; High voltage applications

Introduction

Engineering the surface of battery electrodes is crucial to improve their electrochemical performance as many important reactions happened at this region, including electrolytes decomposition, transition metal dissolution, and Li^+ and e^- combination [1,2]. Many inorganic components have been widely explored as the coating agents, like Al_2O_3 [1,2], ZnO [4], Al_2O_3-doped ZnO [5], TiO_2 [6], and Li_3PO_4 [7]. These coatings improve the cycling stability of battery electrodes by alleviating electrolyte decomposition and reducing the generation of irreversible solid electrolyte interphase (SEI). However, simple metal oxides/phosphates coatings could increase impedance over cycling and decrease rate capability because of their insulating nature towards Li-ions [1]. In addition, most of existing coating techniques require high temperature and/or low vacuum conditions that increase the complexity and cost for the battery manufacturing process [8]. Therefore, exploring novel techniques to engineer battery electrodes warrants further investigate.

Electromagnetic (EM) radiation can aid in synthesizing and crystallizing of both inorganic and organic materials due to their ability to reduce the processing temperature and shorten the processing time [9,10]. One of the most widely studied forms of EM radiation for materials synthesis is microwave radiation (MWR), with frequency in the range of 0.3 and 300 GHz. Compared to conventional furnace-based synthesis methods, the MWR-assisted technique can synthesize inorganic/organic compounds at much shorter times and with higher yields [11-14]. Moreover, the MWR-assisted method generates ceramics with unique crystal structures. For example, Nakamura et al. found that TiO_2 films grown under MWR exposure contain a different phase composition and increased crystallinity compared to those grown at similar temperatures using a furnace-heating method without EM fields [11].

Despite the widespread exploration of the MWR-assisted method in materials synthesis, applying such filed-assisted techniques in lithium ion batteries (LIBs) has not attracted much attention. For example, Kim et al. applied the MWR-assisted method to engineer $FePO_4$ on the surface of $LiCoO_2$ cathode electrode and improved its 4.7 V high voltage cycling stability [15]. However, no follow-up studies were done to explore the effect of other MWR synthesized

ceramics or polymers on the electrochemical performance of $LiCoO_2$ or other cathodes. Nevertheless, many inorganic and organic materials have been synthesized using the MWR-assisted technique [16]. Additionally, many experimental parameters, like microwave power and heating rate, affect the final products during the MWR-assisted synthesis, and will therefore affect the electrochemical performance of battery electrodes. Systematically investigating all these parameters and identifying their optimal combination is not trivial. Accord, further investigations are needed to explore the MWR-assisted technique as a surface engineering technique for battery electrodes.

In this study, we applied MWR to engineer TiO_2 and ZrO_2 on the surface of $LiCoO_2$ electrodes. TiO_2 and ZrO_2 were selected for the first step of study because of their widely applications [17,18]. They have also been proved to improve electrochemical performance of many battery electrodes [19]. We chose $LiCoO_2$ because of its high theoretical capacity and good rate performance. *In-situ* synchrotron x-ray diffraction (XRD) technique was applied to monitor the growth of ZrO_2 and TiO_2 on the surface of $LiCoO_2$ particles. The effect of the coatings on the rate capability and 4.5 V high voltage cycling stability was then investigated. Our study demonstrates that the MWR-assisted technique can become a versatile tool to engineer the surface of battery cathode electrodes. Exploring other coating materials, including both inorganic ceramics and organic polymers, and applying them to advanced cathode materials warrants further investigations for designing next-generation LIBs with high energy and power density as well as extended lifespan.

Materials and Methods

In-situ synchrotron X-ray diffraction characterization

MWR-assisted synthesis experiments were performed using an Anton Paar Monowave 300 reactor operating at 2.45 GHz. The picture of the microwave reactor is shown in Fig. S1 in supporting information (SI). $LiCoO_2$ powder was purchased from MTI cooperation. All other chemicals were purchased from VWR cooperation and used without further purification. Three

in-situ experiments were conducted, (1) MWR-heating of $LiCoO_2$ powder, (2) MWR-assisted synthesis of TiO_2 coatings on $LiCoO_2$ powder, and (3) MWR-assisted synthesis of ZrO_2 coatings on $LiCoO_2$ powder. For the MWR-heating experiment, 200 mg of $LiCoO_2$ powder was dispersed in a 5 mL tetraethyl glycol (TEG) solution and heated up to 250^oC at the rate of 1.5^oC/min (the slowest rate that can be achieved by the microwave reactor), held at that temperature for 10 minutes, and cooled to 55^oC. The solution was stirred at 650 rpm to avoid hotspot formation. For the other experiments, where TiO_2 and ZrO_2 coatings were synthesized on $LiCoO_2$ powder, sol-gel solutions based on titanium(IV) butoxide and zirconium(IV) tert-butoxide were used as TiO_2 and ZrO_2 precursors, respectively [19]. The sol-gel was mixed with TEG in the ratio of 1:4 by volume. 200 mg of $LiCoO_2$ powder was dispersed in a total of 5 ml precursor solution, which was then heated in the microwave reactor using identical experimental conditions as the MWR-heating experiment.

Fig. S1 shows a schematic of the i*n-situ* synchrotron XRD experiments that were conducted at the 6-ID-D beamline at the Advanced Photon Sources, Argonne National Laboratory. A monochromatic X-ray beam of energy 80 keV was used for diffraction, which allows for X-ray transmission through the thick walls of glass vials. A 2-D Perkin Elmer amorphous silicon area detector with Cesium Iodide scintillator was used to collect 2D diffraction patterns. Because of the high absorption of X-rays by glass vials, an acquisition rate of 1 minute was used for data collection. This rate achieved an acceptable signal-to-noise ratio; the ceramic oxide diffraction peaks could be distinguished from the background signal caused by the glass vial and solution while considering the temporal resolution of the chemical reaction. The microwave reactor was modified to include inlet and outlet ports allowing X-rays to pass through and reach the glass vial. Fit2D was utilized to convert 2D detector images to intensity-2 theta angle relationships. High order polynomial functions were applied to remove the solution and glass vial background via MATLAB [21,22]. The remaining peaks were then identified and individually fit to Gaussian peaks to obtain peak locations, intensities, and full-width at half maxima (FWHM).

MWR-assisted method to synthesize TiO_2 and ZrO_2 coating on $LiCoO_2$ surface for LIB electrodes

To engineer TiO_2 and ZrO_2 on the surface of $LiCoO_2$ powder, 500 mg of $LiCoO_2$ powder was dispersed in a 12 ml solution comprising of 9 ml TEG and 3 ml sol-gel solution. TiO_2 synthesis was performed using experimental conditions of 150^{o}C - 200 W - 10 min - 1 min, where 150^{o}C represented the maximum temperature, 200 W was the maximum microwave power applied, 10 min was the heating time to reach the maximum temperature, and 1 min was the hold time at the maximum temperature [11]. The vial was cooled down to 55^{o}C by forced air cooling after the experiment. The experimental conditions for MWR-assisted ZrO_2 synthesis were 225^{o}C - 200 W - 30 min - 1 min [23]. The obtained powder was washed three times with deionized water and then dried at 80^{o}C in a vacuum chamber overnight. The dried powder was subsequently annealed at 750^{o}C for 6 hours in air, followed by air cooling to room temperature.

Material characterization

Transmission electron microscopy (TEM) imaging was used to characterize the TiO_2 and ZrO_2 coatings on $LiCoO_2$ powder. The synthesized powder was dispersed in ethanol, dropped onto TEM grids and dried overnight before being loaded for imaging. TEM characterization was performed using a FEI Talos F200X operated at 200 kV. Energy dispersive X-ray spectroscopy (EDS) data was collected by ChemiSTEM technology (X-FED and SuperX EDS) using four silicon drift detectors.

X-ray photoelectron spectroscopy (XPS) measurements were done on a Thermo Fisher ESCALAB 250Xi with an X-ray source of monochromatized Al K α radiation (1486.7 eV). The base pressure was 10^{-8} Pa, and the spot diameter was 600 μm. Five survey scans with a step size of 1.0 eV were collected, followed by ten high-resolution scans with a step size of 0.1 eV for target elements. The obtained XPS spectra were analyzed by AVENTAGE software with the following parameters: FWHM (eV) = 0.5:3.5 and Lorentzian/Gaussian of 0.3. In the XPS depth profiling analysis, Ar^+ ion beam was applied on an area of 3 mm *3 mm for the etching process, followed by XPS data collection for specific elements. The Ar^+ gun was

operated at 3 keV and the etching time was 15 seconds for each step. A total of 50 steps were applied on each sample for the depth profiling analysis.

The weight percentages of Co, Ti, and Zr in $LiCoO_2$ powder were measured by inductively coupled plasma mass spectrometry (ICP-MS, Agilent Technologies 7700 Series). Briefly, 7.3 mg of TiO_2-coated $LiCoO_2$ powder or 9.6 mg of ZrO_2-coated $LiCoO_2$ powder was added into 15 ml centrifuge tube containing 5 ml HCl (37%). The tubes were sealed and rotated on an end-over-end rotator (30 rpm) overnight. Then the solution was diluted by 2000 times. 6 ml of the solution was filtered through a 0.45 μm filter, and 0.2 ml of trace metal grade HNO_3 (69%) was added to acidize the solution. Mixed standards of 0, 10, 20, 50, 100, 250, and 500 ppb for different elements with the same percentage of HNO_3 (~ 5%) as the samples were used for calibration.

To study the Co dissolution from $LiCoO_2$ electrodes after cycling, coin cells were disassembled in an argon-filled glove box with O_2 and H_2O level below 0.5 ppm. All components were immersed in 10 ml dimethyl carbonate (DMC) for three days. 2 ml of the solution was then diluted in 6 ml HNO_3 (65%). The mixed solution was heated to 120^{o}C in a vacuum chamber until all liquid disappeared. The remaining white/yellow powder was collected and dissolved in 10 ml deionized water, followed by 30 min of ultrasonic treatment. Finally, 6 ml solution was filtered through a 0.45 μm filter and 0.2 ml HNO_3 (70%) was added to the solution before conducting the ICP-MS measurement.

Electrode preparation, coin cell fabrication, and testing

$LiCoO_2$ powder with and without the TiO_2/ZrO_2 coating was mixed with carbon black and polyvinylidene fluoride in N-methyl pyrrolidone with a ratio of 8:1:1 by weight. The slurry was then spread on an aluminum foil current collector and dried in a vacuum chamber at 110^{o}C overnight to remove the solvent and moisture. 14 mm diameter cathode disks were punched and collected in glass bottles, with a typical mass loading of 4 − 5 mg. CR-2016 type coin cells were fabricated using these disks as the cathode and lithium chips as the anode. Celgard separators and lithium chips were purchased from MTI Corporation, while electrolytes were

purchased from Sigma Aldrich. The electrolyte was ethylene carbonate/ethyl methyl ethyl carbonate (50/50, v/v) containing 1 M $LiPF_6$. The entire assembly process was carried out in an argon-filled glovebox with O_2 and H_2O level maintained below 0.5 ppm.

Electrochemical performance of $LiCoO_2$ electrodes was measured using Biologic VMP3 (Bio-Logic Science Instruments) and LAND battery cyclers (LAND Electronics Co., Ltd.). After assembling, all cells went through a formation process consisting of three continuous cycles at C/10 (1C = 145 mA/g) within 3.0 – 4.2 V at room temperature. Rate capability was studied by charging cells at C/3 using constant current (CC) – constant voltage (CV) protocol, followed by different discharging rates, including C/10, C/3, 1C, 2C, 5C, and 10C. The cut-off current during the CV charging process was C/100 to ensure that all cells were discharged at the same status. Galvanostatic intermittent titration technique (GITT) measurement was conducted by applying a 30 min galvanostatic charge/discharge pulse (C/10) followed by a 2 h relaxation. Electrochemical impedance spectroscopy (EIS) was tested at room temperature. Before the EIS measurement, cells were charged to 4.0 V using a CC-CV protocol with C/100 as the cut-off current during the CV process. The impedance was then potentiostatically measured by applying an AC voltage of 10 mV amplitude over the frequency range of 100 kHz to 10 mHz. High voltage cycling test was conducted at room temperature by cycling cells at C/2 within the voltage range of 3.0 – 4.5 V using a CC protocol for both charging and discharging processes.

Results

Material characterization

Many microwave processing parameters affect the final synthesized products, including maximum temperature, maximum microwave power, heating rate, and hold time at the maximum temperature. The maximum temperature was determined based on the results from the *in-situ* synchrotron XRD experiment, as shown in Figure 1. Figure 1a shows the temperature and power profiles of the microwave system during the MWR-assisted heating of $LiCoO_2$. The corresponding two-dimensional contour plot for the structure of $LiCoO_2$ powder is displayed in Figure 1b. At around 115 minute, we found significant shifts of two-theta values

in the XRD pattern, suggesting a new phase formed because of the microwave heating. Fig. S2 suggests the new phase is cubic CoO [24]. The formation of cubic CoO started at 230₀C. Therefore, the maximum temperature for engineering TiO_2 and ZrO_2 coatings on the surface of $LiCoO_2$ was set below 230₀C to avoid any such phase transformation of $LiCoO_2$ during the MWR processing. Although other parameters, like the heating rate and the hold time, affected the synthesized TiO_2 and ZrO_2, these parameters were not systematically studied and were chosen based on empirical trials [20]. Optimizing these parameters is not trivial and warrants further investigations.

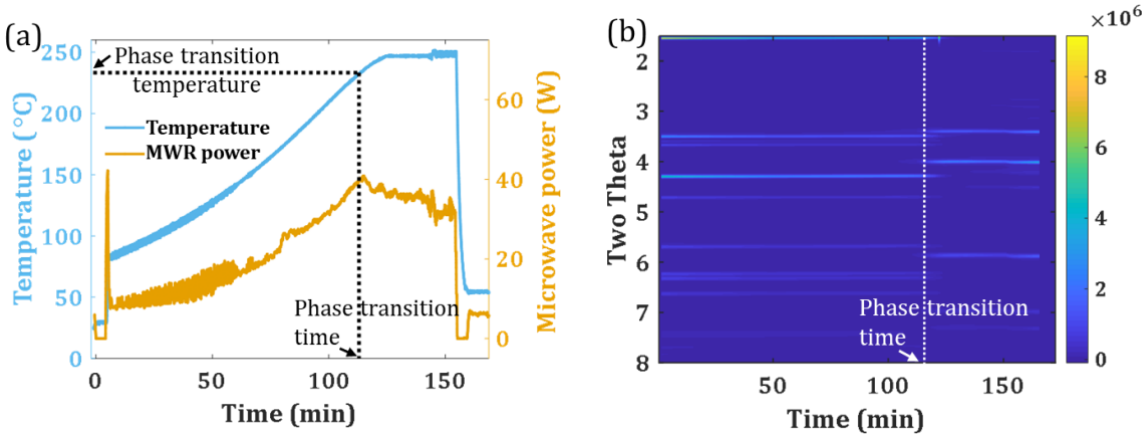

Figure 1. In-situ synchrotron X-ray diffraction (XRD) results. (a) Temperature and power profile during in-situ synchrotron XRD experiment for $LiCoO_2$ powder in TEG solution. (b) The evolution of 2θ values for the diffraction pattern during in-situ XRD experiment.

TiO_2 and ZrO_2 coatings on $LiCoO_2$ were studied using TEM, scanning transmission electron microscopy (STEM), EDS, and XPS. It has been reported that localized hot spots can form in $LiCoO_2$ due to MWR absorption, which may promote TiO_2/ZrO_2 nucleation [15]. Figure 2a, b, c shows TEM image of a pristine $LiCoO_2$ particle, a TiO_2-coated $LiCoO_2$ particle, and a ZrO_2-coated $LiCoO_2$ particle, respectively. No obvious films could be identified in Figure 2b, while a thin layer is shown in Figure 2c. However, the thin layer was proven to be carbon rather than ZrO_2, as shown in Fig. S3. The EDS results in Figure 2d, e show that Ti is uniformly distributed on the surface of $LiCoO_2$ powder, while Zr nucleated at a few regions on the edge of $LiCoO_2$ particles. Three different locations were tested to statistically study the distribution of Ti and Zr on $LiCoO_2$ particles, as displayed in Fig. S4 (SI). The result shows that Ti uniformly distributed on the surface of $LiCoO_2$ particles in all cases except one particle (Fig. S4c), while

Zr nucleated at a few regions on the edge of $LiCoO_2$ particles in all cases. To further examine the existence of TiO_2 and ZrO_2, XPS was collected on both TiO_2-coated and ZrO_2-coated $LiCoO_2$ samples, as shown in Fig. S5. A Ti 2p3/2 peak at 458.4 eV and a Zr 3d5/2 peak at 181.9 eV could be identified, proving the existence of Ti and Zr on the surface of TiO_2-coated and ZrO_2-coated $LiCoO_2$ powder, respectively. Based on these results, we demonstrate that TiO_2 and ZrO_2 were successfully synthesized on the surface of $LiCoO_2$ powder using the MWR-assisted technique.

Table S1 shows that the weight percentage of Co in both TiO_2-coated $LiCoO_2$ and ZrO_2-coated $LiCoO_2$ powder was very close to the theoretical value of Co in $LiCoO_2$ (60.2%). Additionally, the weight percentages of Ti and Zr in the powder were less than 1%. This result suggests that the weight percentages of TiO_2 and ZrO_2 in these TiO_2 and ZrO_2-coated $LiCoO_2$ powders were negligible. Therefore, the TiO_2 and ZrO_2 coatings should have little effect on the specific capacity of $LiCoO_2$ electrodes.

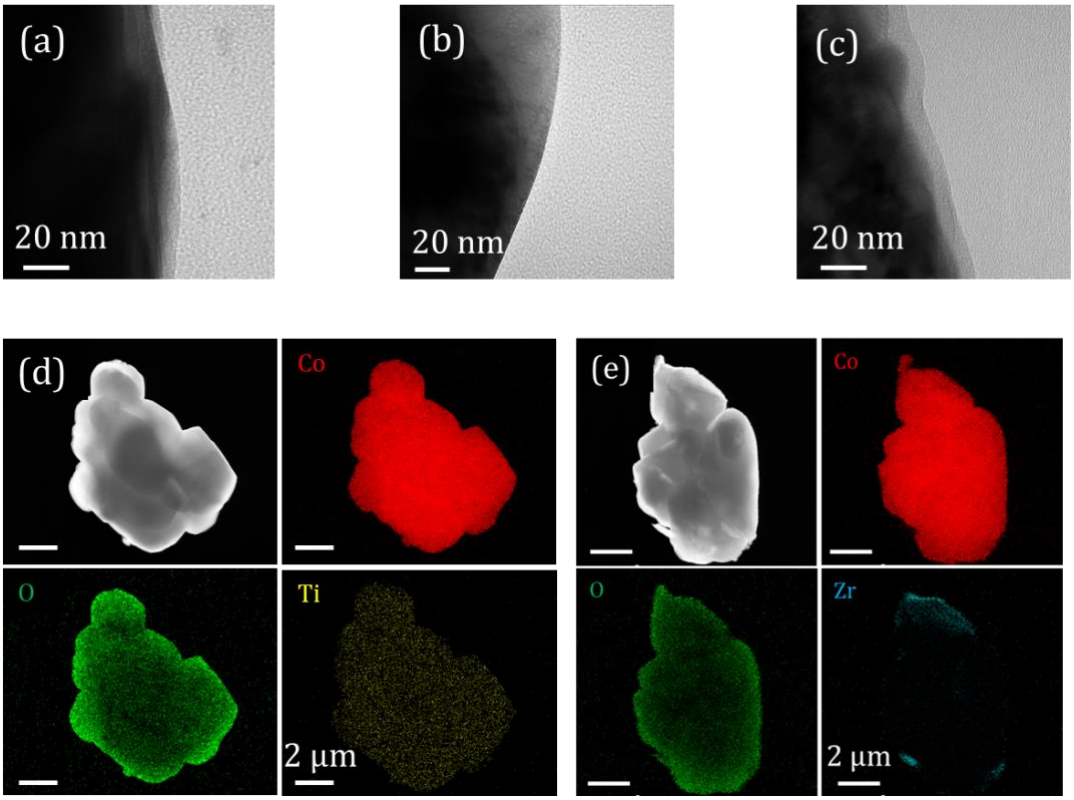

Figure 2. TEM images of (a) a pristine $LiCoO_2$ particle, (b) a TiO_2-$LiCoO_2$ particle and (c) a ZrO_2-$LiCoO_2$ particle. (d) STEM image and EDS of a TiO_2-$LiCoO_2$ particle. (e) STEM image and EDS of a ZrO_2-$LiCoO_2$ particle.

Influence of MWR-synthesized TiO_2/ZrO_2 coatings on rate capability of $LiCoO_2$ electrodes

Figure 3 illustrates the effect of TiO_2 and ZrO_2 coatings on the rate capability of the $LiCoO_2$ electrode. The ZrO_2 coating had little effect on the rate capability, while the TiO_2 coating improved rate capability. The effect of coatings on the rate performance becomes more obvious at high rate. Figure 3a indicates that the discharge capacity of the $LiCoO_2$ electrode increased by around 50% (from 60 to 90 mA h g^{-1}) after the TiO_2 coating at 10C). In comparison, the ZrO_2 coating did not affect the discharge capacity of the $LiCoO_2$ electrode in the rate range we measured. Figure 3b compares discharge curves of different $LiCoO_2$ electrodes at C/10, 1C, and 10C. The discharge curves of the ZrO_2-coated $LiCoO_2$ and the pristine $LiCoO_2$ electrode almost overlapped each other at all the three C-rates, while the TiO_2-coated $LiCoO_2$ electrode behaved differently. At low C-rates (C/10 and 1C), the discharge curves of the TiO_2-coated $LiCoO_2$ electrode overlapped the pristine $LiCoO_2$ electrode at the initial stage of the discharging. However, the voltages stayed much higher when it closed to the end of the discharging before quickly dropped to 3.0 V. At the high C-rate (10C), the TiO_2-coated $LiCoO_2$ electrode showed higher voltage (~ 0.2 V) during the entire discharging process and 40 mA h g^{-1} larger specific capacity than the pristine $LiCoO_2$ electrode.

The rate performance of the $LiCoO_2$ electrode could be affected by the kinetics of lithium transport in the electrode. We applied GITT to study the effect of TiO_2/ZrO_2 coating on the transport of lithium in $LiCoO_2$. The details of the measurement process can be found in Fig. S6, which suggests that the diffusion coefficient of lithium in $LiCoO_2$ varied little in the voltage range of 4.0 – 4.4 V. Additionally, the diffusion coefficients during the charge and discharge processes were similar in value. Therefore, we only measured the diffusion coefficient of lithium in $LiCoO_2$ during the charge process at around 4.0 V for TiO_2-coated and ZrO_2-coated $LiCoO_2$ electrodes. Figure 3c compares the lithium diffusion coefficient in the three types of $LiCoO_2$ electrodes. The results suggest that the diffusion coefficients were in the same order of magnitude. However, the TiO_2-coated $LiCoO_2$ electrode had slightly higher diffusion coefficients (~$5.5*10^{-12}$ cm^2S^{-1}) compared with the pristine $LiCoO_2$ electrode (~$4.0*10^{-12}$ cm^2S^{-1}). This agreed with the improved discharge performance of the TiO_2-coated $LiCoO_2$

electrode seen in Figure 3b. Figure 4 compares the diffusion coefficient of Li in different $LiCoO_2$ electrodes measured from cyclic voltammetry (CV). The voltage swapping rate was varied from 0.2 to 1.0 mV/s, during which the current was monitored. Figure 4 suggests that the peak current (I_p) linearly increased with the square root of voltage swapping rate ($v^{1/2}$). By applying Randles-Sevcik equation, we calculated the diffusion coefficient of Li in different $LiCoO_2$ electrodes [25]. The result suggests that both TiO_2 and ZrO_2 coatings increased the diffusion coefficient of Li. Because the order of magnitude in the difference between these diffusion coefficients was small, more investigations are needed before drawing a clear conclusion.

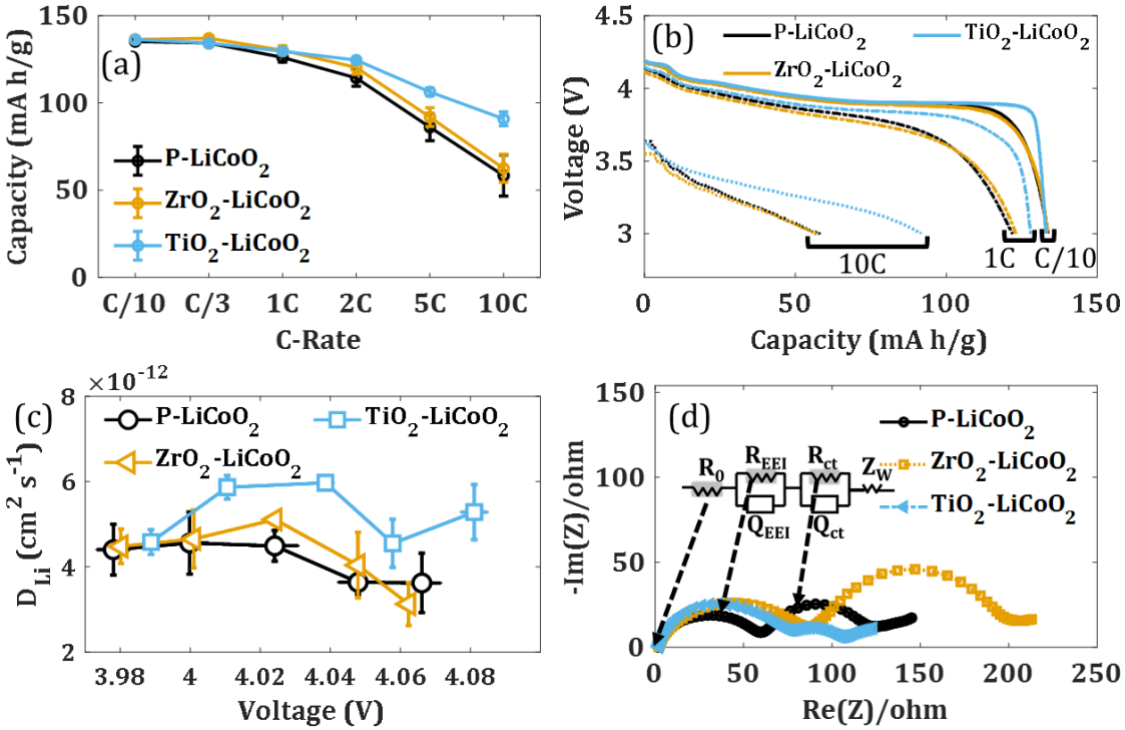

Figure 3. Rate performance of different $LiCoO_2$ electrodes. (a) Specific capacity of $LiCoO_2$ electrodes with respect to discharging rate. Three cells were tested for each case and the result was averaged from all cells. (b) Comparison of discharge curves of $LiCoO_2$ electrodes at C/10, 1C, and 10C. (c) Diffusion coefficient of Li in $LiCoO_2$ during lithiation (charging) at around 4.0 V for different electrodes using GITT method. (d) EIS plots of different $LiCoO_2$ electrodes. The figure inset shows a second-order ECM that is used to fit the impedance.

EIS measurements were also conducted to study the effect of these coatings on the impedance of the $LiCoO_2$ electrode. The impedance of a coin cell is very sensitive to the fabrication process. Cells with the same type of $LiCoO_2$ electrode could have different impedance values, as shown in Fig. S7 (SI). However, the overall trend suggests that the TiO_2 coating reduced the

impedance while the ZrO_2 coatings increased the impedance, as shown in Figure 3d. To quantitatively analyze these results, the impedances were fitted using a second order equivalent circuit model (ECM), as shown in the inset in Figure 3d. The R_0 represents the ohmic resistance, the R_{EEI} and Q_{EEI} represent the resistance and the phase constant element of the EEI layer, the R_{ct} and Q_{ct} represent the resistance and the phase constant element charge-transfer process. The fitted results in Table S2 suggests that the ZrO_2 and TiO_2 coatings had little effect on R_0, but they increased the R_{EEI}. Additionally, the ZrO_2 coating increased the R_{ct}, while the TiO_2 coating decreased the resistance. The effect of different metal oxides coatings on the impedance of the $LiCoO_2$ electrode has been reported before [3-5]. The slightly increased R_{EEI} was attributed to either poor Li^+ transport through the EEI layer after the TiO_2/ZrO_2 coating or the formation of a thicker EEI layer because of the coating. The decreased/increased R_{ct} of the $LiCoO_2$ electrode after the TiO_2/ZrO_2 coating could be attributed to different side products on the surface of the electrode, which was generated by reactions between the coatings and electrolytes. The side products could affect the de-solvation process at the interface of EEI and electrolyte as well as affect the charge-transfer process at the interface of EEI and electrolyte, leading to different R_{ct}.

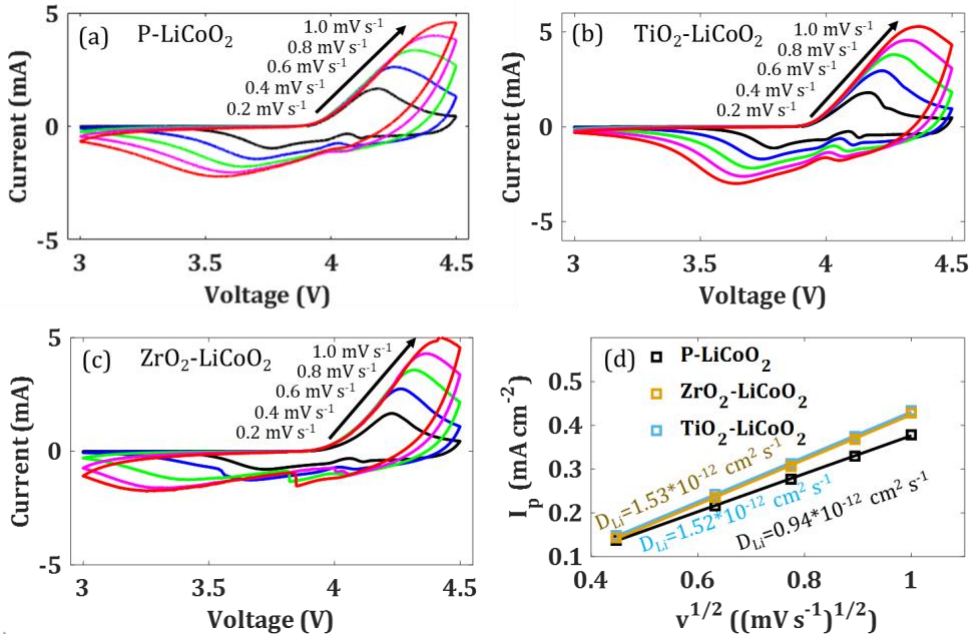

Figure 4. Cyclic voltammetry of (a) pristine $LiCoO_2$, (b) TiO_2 coated $LiCoO_2$, and (c) ZrO_2-coated $LiCoO_2$ at different scan rates. (d) The evolution of peak current with respect to scan rate for different samples. Both TiO_2 and ZrO_2 coating slightly increase the diffusion coefficients of Li in $LiCoO_2$.

Influence of MWR-synthesized TiO_2/ZrO_2 coatings on cycling stability of $LiCoO_2$ electrodes

The 4.5 V high voltage cycling stability of the $LiCoO_2$ electrode was largely improved by the TiO_2 and ZrO_2 coatings. Figure 5a compares the evolution of specific capacity for the three types of $LiCoO_2$ electrodes during the cycling test. The result shows that the TiO_2 and ZrO_2 coatings significantly reduced the rate of capacity degradation. The ZrO_2 coating improved the capacity remaining from 52.8% to 81.9% after 40 cycles, while the TiO_2 coating improved it to 84.4%. Such improvement is battery than many of existing studies, especially for the TiO_2 coating (Table S3). The middle voltage of a cell is the voltage at the half of the discharge capacity, which represents the kinetic properties of the cell. Figure 5b shows that the middle voltage of the pristine $LiCoO_2$ electrode decreased from 3.964 to 3.232 V after 40 cycles, while the ZrO_2-coated $LiCoO_2$ electrode decreased from 3.968 to 3.878 V, and TiO_2-coated $LiCoO_2$ electrode decreased from 3.968 to 3.924 V. Thus, the TiO_2 and ZrO_2 coatings reduced the capacity degradation rate and protected the kinetics of the $LiCoO_2$ electrode during the high voltage cycling test.

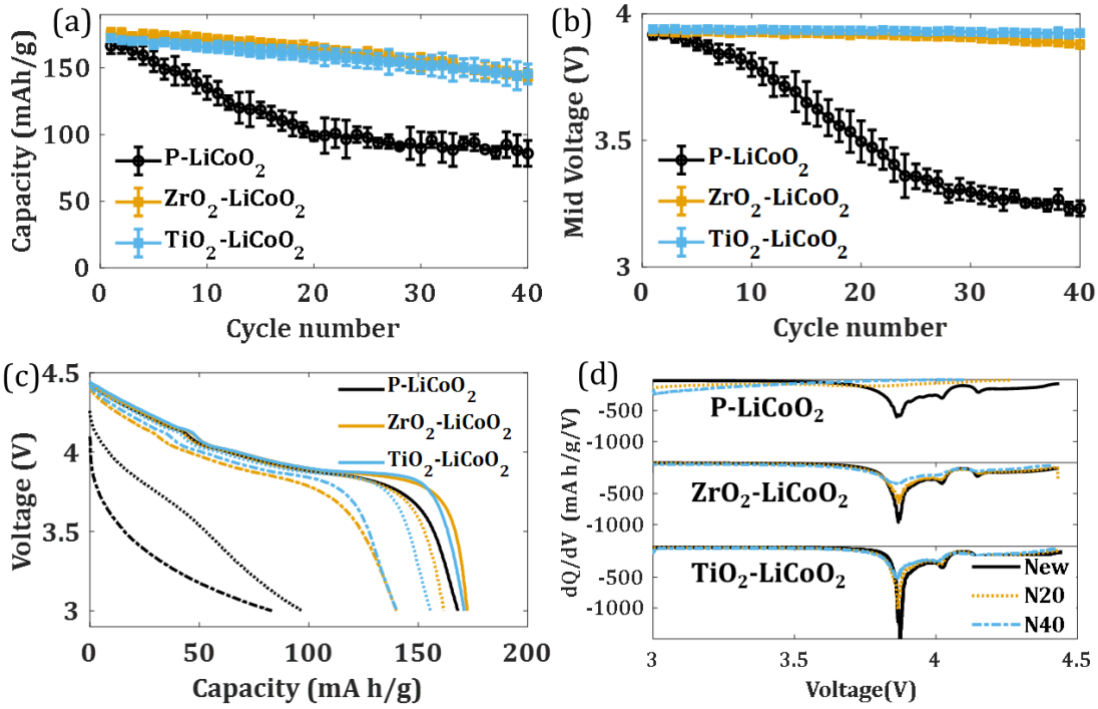

Figure 5. High voltage (4.5 V) cycling stability of different $LiCoO_2$ electrodes. (a) The capacity degradation of $LiCoO_2$ electrodes. Three cells were tested for each type of electrode and the distribution is shown in the error bar. (b) The evolution of the middle voltage for different $LiCoO_2$ electrodes. (c) Discharge curves (C/2) of the

$LiCoO_2$ electrodes at new status, after 20 cycles, and after 40 cycles. (d) Incremental capacity analysis (ICA) for the discharge curves of $LiCoO_2$ electrodes in plot (c).

The effect of the TiO_2 and ZrO_2 coatings on the cycling stability of the $LiCoO_2$ electrode was further investigated by comparing and analyzing discharge curves, as shown in Figure 5c, d. Figure 5c displays the discharge curves of the three types of $LiCoO_2$ electrodes at different aging statuses. The discharge curves of the pristine $LiCoO_2$ electrode showed a large drop in voltage and specific capacity after 20 (N20) and 40 cycles (N40). Moreover, the discharge plateaus almost disappeared in the discharge curves on N20 and N40. However, both the TiO_2 and ZrO_2 coatings reduced the decrease of the voltage and the specific capacity of the $LiCoO_2$ electrode after 20 and 40 cycles. Additionally, the coatings maintained the discharge plateaus after the cycling test. Figure 5d compares the incremental capacity analysis (ICA) curves of the three $LiCoO_2$ electrodes at different aging statuses. An ICA peak corresponds to a plateau in a discharge curve, which represents a phase transition process in the $LiCoO_2$ electrode. Before the cycling test, three peaks could be identified for all $LiCoO_2$ electrodes at around 4.15, 4.03, and 3.87 V. The intensity of a peak could be affected by the cathode material and the homogeneous current distribution within the electrode. The higher ICA peak at 3.87 V in the TiO_2-coated $LiCoO_2$ electrode suggests that the TiO_2 coating improved the homogeneity of current distribution in the $LiCoO_2$ electrode. This further agreed with the better rate performance of the TiO_2-coated $LiCoO_2$ electrode seen in Figure 3. After 20 and 40 cycles, all the ICA peaks of the pristine $LiCoO_2$ electrode disappeared, indicating either $LiCoO_2$ particles were destroyed that led to no phase transformations during the discharge process or largely inhomogeneous current distribution occurred in the electrode during discharge. In comparison, the ICA curves of both the ZrO_2-coated and the TiO_2-coated $LiCoO_2$ electrodes still showed three ICA peaks after 20 and 40 cycles. However, the locations of these peaks shifted to lower voltages and the intensities decreased after the cycling test, indicating the increase of cell resistance and the inhomogeneity of current distribution in these electrodes.

EIS measurements show that the TiO_2 and ZrO_2 coatings reduced the increase of the overall impedance of the $LiCoO_2$ electrode during the cycling test. Figure 6a compares the impedances of the three types of $LiCoO_2$ electrodes after 40 cycles. The charge transfer resistance (R_{ct}) in

the pristine $LiCoO_2$ electrode became much larger than that in the TiO_2 and ZrO_2-coated $LiCoO_2$ electrodes. This phenomenon has been reported inhibit the increase of R_{ct} in $LiCoO_2$ electrodes during cycling tests [26]. A second order ECM was applied to quantitatively analyze the impedance and the fitted results are listed in Table S2. The R_{ct} of the pristine $LiCoO_2$ increased by almost two orders of magnitude (80 times) after the cycling test, while the R_{ct} of the ZrO_2-coated and TiO_2-coated $LiCoO_2$ only increased by around 2.5 and 1.5 times, respectively. This might be from the formation of a passivation film on the surface of $LiCoO_2$, like LiF, Li_xPF_y, and $Li_xPF_yO_z$-type of compounds, which limited the charge-transfer process of Li^+ at the cathode-electrolyte interface [27,28]. The slow increase of R_{ct} in the TiO_2/ZrO_2-coated $LiCoO_2$ electrode suggested that the TiO_2 and ZrO_2 coatings could inhibit the formation of these compounds. Table S2 also suggests that the R_0 did not increase after the cycling test for all the three $LiCoO_2$ electrodes, indicating that the electron transport pathways were maintained in these electrodes during the cycling test. Additionally, the R_{EEI} slightly decreased for all the three types of $LiCoO_2$ electrodes. The decreased R_{EEI} could be caused by the formation of cracks on the $LiCoO_2$ electrodes during the cycling test that increased the total surface area of the electrodes [27].

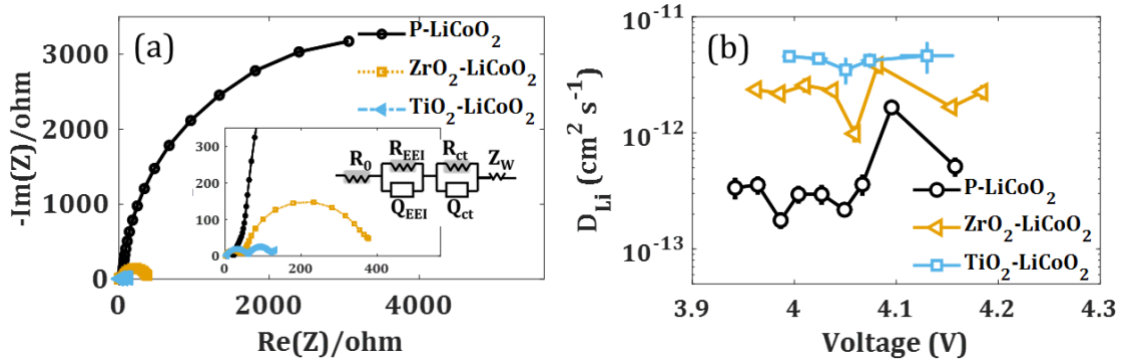

Figure 6. Kinetics of $LiCoO_2$ electrode after the cycling test. (a) EIS results for the three types of $LiCoO_2$ electrodes. (b) The diffusion coefficient of Li in $LiCoO_2$ electrodes.

GITT data showed that the TiO_2 and ZrO_2 coatings helped maintain the kinetics of lithium transport in the $LiCoO_2$ particles during the cycling test. Figure 6b shows that the TiO_2-coated $LiCoO_2$ electrode had the highest lithium diffusion coefficient (~4.2*10-12 cm2S-1) after cycling, which changed little from its initial status (~5.5*10-12 cm2S-1). Similarly, the lithium diffusion coefficient in the ZrO_2-coated $LiCoO_2$ electrode decreased little after cycling (from ~4.0*10-12

cm^2S^{-1} to ~$2.3*10^{-12}$ cm^2S^{-1}). In comparison, the lithium diffusion coefficient in the pristine $LiCoO_2$ decreased by more than an order of magnitude after the cycling test (from ~$4.0*10^{-12}$ to ~$2.3*10^{-13}$ cm^2S^{-1}). This result suggests that the pristine $LiCoO_2$ particles went through severe damage during the cycling test, such as surface reconstruction caused by Co dissolution and channel blocking caused by the change of crystal structure on the surface [29]. These damages were reduced, if not eliminated, by the TiO_2 and ZrO_2 coatings according to the well-maintained lithium diffusion coefficients seen in the TiO_2/ZrO_2-coated $LiCoO_2$ electrodes.

The TiO_2 and ZrO_2 coating also reduced the Co dissolution from the $LiCoO_2$ electrode into the electrolyte, which is considered as one of the mechanisms for capacity degradation of $LiCoO_2$ during cycling [30]. By applying the treatment described in the methodology section, we measured the concentration of Co element in the final electrolyte solution using ICP-MS technique. After the cycling test, the ratio of the dissolved Co to the total mass of the $LiCoO_2$ electrode was 0.76%, 0.12%, and 0.06% for the pristine $LiCoO_2$ electrode, the TiO_2-coated $LiCoO_2$ electrode, and the ZrO_2-coated $LiCoO_2$ electrode, respectively. Thus, the TiO_2 and ZrO_2 coating inhibited the dissolution of Co, which further explained the improved capacity remaining of the $LiCoO_2$ electrode after these coatings.

Discussion

It has be reported that the degradation of $LiCoO_2$ during cycling (below 4.5 V) is attributed to surface degradation effects rather than bulk degradation [31,32]. This suggests the degradation rate could be related to the surface area of $LiCoO_2$ particles, i.e. the radius of the particle. Figure 7 summarizes the capacity fade rate of $LiCoO_2$ cycled at 4.5 V in recent papers. The figure suggests that the capacity fade rate increases with the decrease of the primary particle size. In our study, the $LiCoO_2$ particle size is 2 μm and the degradation rate of pristine $LiCoO_2$ is 1.18%/cycle. Our experiment data follows the trend of $LiCoO_2$ capacity fade rates reported in recent studies.

Additionally, our study shows that the degradation rate of $LiCoO_2$ is largely reduced by TiO_2 and ZrO_2 coatings. Table 1 compares the effect of TiO_2 and ZrO_2 coatings on $LiCoO_2$ 4.5 V

cycling performance via different techniques. Compared to existing literatures, the ZrO_2 coated $LiCoO_2$ in our study shows comparable cycling performance, while the TiO_2 coated $LiCoO_2$ shows much better cycling stability.

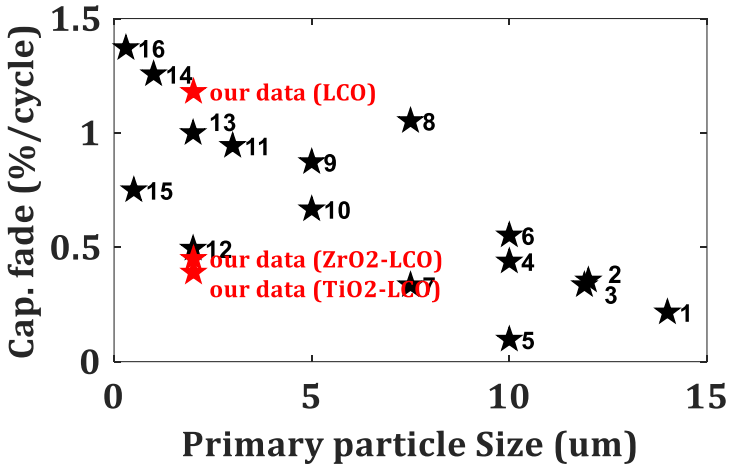

Figure 7. Comparison 4.5 V high voltage cycling performance of pristine LiCoO2 with different particle sizes. Data is collected from recently published paper, as listed in Table S3. Our experiment data is highlighted by red, where LCO stands for pristine LiCoO2 electrode and ZrO2/TiO2-LCO stands for ZrO2/TiO2-coated LiCoO2 electrode.

Table 1. Comparison of $LiCoO_2$ cycling stability at 4.5 V with TiO_2 and ZrO_2 coatings

Study	Coating	Technique	Cut-off voltage	Capacity fade rate improvement
Ref. [33]	TiO2	ALD	4.5 V	0.60% → 0.57%/cycle
Ref. [6]	TiO2	Sputtering	4.5 V	0.55% → 0.25%/cycle
Ref. [34]	TiO2	sol-gel synthesis	4.5 V	2.4% → 1.40%/cycle
This study	**TiO_2**	**MWR**	**4.5 V**	**1.18% → 0.39%/cycle**
Ref. [35]	ZrO2	Furnace Heating	4.5 V	2.63% → 0.50%/cycle
Ref. [36]	ZrO2	heat treatment	4.5 V	0.63% → 0.16%/cycle
This study	**ZrO2**	**MWR**	**4.5 V**	**1.18% → 0.45%/cycle**

XPS is a surface-sensitive spectroscopic technique that reveals not only the composition of the sample surface, but also the oxidation states of different elements present on the sample surface. Accordingly, we applied XPS to investigate the effect of the TiO_2 and ZrO_2 coatings on the electrochemical performance of the $LiCoO_2$ electrode. The TiO_2 coating affected the oxidation status of Co on the surface of $LiCoO_2$, while the ZrO_2 coating had little effect. Figure

8a compares the binding energy of Co 2p peaks in $LiCoO_2$ powder before and after the TiO_2/ZrO_2 coating via the MWR-assisted synthesis, followed by the heat treatment. The TiO_2-coated $LiCoO_2$ powder before the heat treatment is also shown for comparison. Two XPS peaks at 780.0 eV and 780.46 eV were assigned to Co 2p3/2. The lower binding energy was from Co^{3+} in $LiCoO_2$, while the higher binding energy was from Co^{2+} in $Co(OH)_2$ that formed on the surface of $LiCoO_2$ during air exposure [28]. The results show that the ZrO_2 coating did not affect the binding energies of Co 2p3/2, while the TiO_2 coating increased the Co^{3+} peak from 780.0 to 780.18 eV and increased the Co^{2+} peak from 780.46 to 780.63 eV. The increased binding energies for Co 2p3/2 were not found in the TiO_2-coated $LiCoO_2$ powder before the heat treatment, suggesting the heat treatment rather than the microwave processing affected the surface state of $LiCoO_2$ in the TiO_2-coated $LiCoO_2$ powder. The little effect of the microwave processing on $LiCoO_2$ powder was also supported by analyzing the *in-situ* XRD data in Fig. S9. The data suggests that the lattice parameter of $LiCoO_2$ did not change during the MWR-assisted synthesis of TiO_2 on the surface of $LiCoO_2$.

Figure 8b compares the binding energy of Ti 2p in the TiO_2-coated $LiCoO_2$ powder before and after the heat treatment. The results display that the Ti 2p2/3 peak decreased from 458.40 to 458.06 eV after the heat treatment, suggesting that the heat treatment promoted interactions between Ti and Co on the surface of $LiCoO_2$. One possible mechanism is that Ti diffused into the surface of $LiCoO_2$ lattice by either forming Ti interstitial or substituting Co [37]. This process affected the oxidation state of Co and Ti atoms and thus changed the binding energies of Co 2p3/2 in $LiCoO_2$ and Ti 2p3/2 in TiO_2. However, the atomic radius of Zr (230 pm) is much bigger than Ti atom (147pm), making Zr atom harder to diffuse into $LiCoO_2$ lattice. We believe that such a mechanism could also explain the different effects of the TiO_2 and ZrO_2 coatings on the diffusion coefficient of lithium in $LiCoO_2$ (Figure 3c) as well as the rate capability of $LiCoO_2$ electrodes (Figure 3a, b).

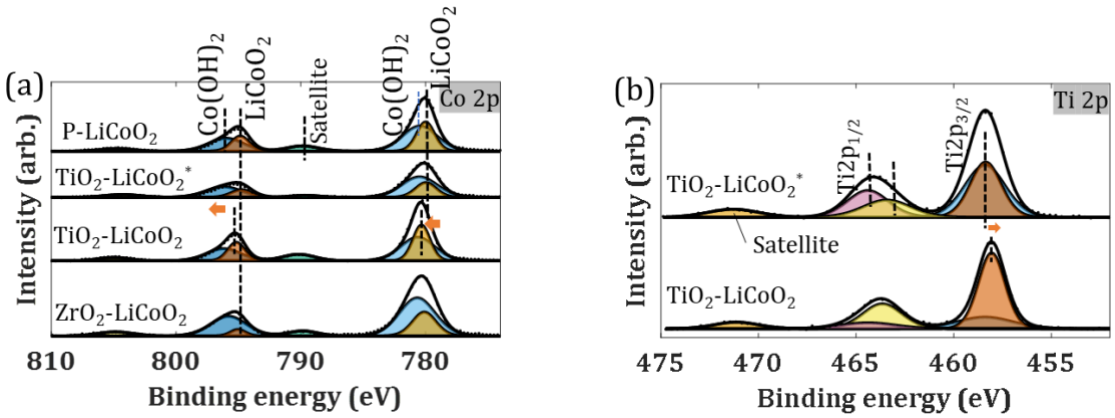

Figure 8. X-ray photoelectron spectroscopy (XPS) measurement for different samples. (a) XPS spectroscopy of Co 2p in pristine $LiCoO_2$, TiO_2-coated $LiCoO_2$, and ZrO_2-coated $LiCoO_2$. (b) The XPS spectroscopy of Ti 2p in TiO_2-coated $LiCoO_2$ electrodes. The TiO_2-$LiCoO_2$ represents the TiO_2-coated $LiCoO_2$ without heat treatment. Measurement data (dots) are fitted by several individual spectra (colored regions). The combined spectra from these color shaded regions is shown as an envelope that matches well with experimental data (dots).*

To understand the improved high voltage cycling stability in the TiO_2-coated $LiCoO_2$ electrode, XPS depth profiling was conducted for $LiCoO_2$ electrodes with and without the TiO_2 coating, after 40 cycles. The results are shown in Figure 9. The F 1s curve at 0s (no etching) could be roughly allocated into two peaks. The one at higher binding energy (~ 688 eV) was from fluoroorganic species, like C-F in PVDF, P-F in PF_6-, as well as other organic side products that contain fluoride, while the one at lower binding energy (~ 685 eV) was attributed to LiF [28]. Compared with the fluoroorganic species peak, the Li-F peak in the pristine $LiCoO_2$ electrode was very weak and only showed up after 450 seconds of etching. Since many reports show that the passive film formed on battery electrodes is composed of an inner inorganic layer and an outer organic layer, the weak Li-F peak at 0s indicated the formation of a relatively thick organic passivation film on the surface of the pristine $LiCoO_2$ after 40 cycles [38,39].

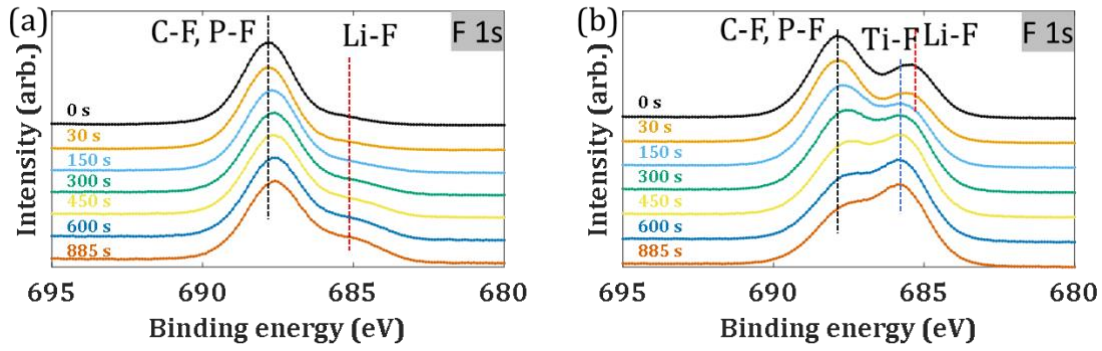

Figure 9. XPS measurement of F 1s binding energies for (a) pristine $LiCoO_2$ electrode, and (b) TiO_2-coated $LiCoO_2$ electrode after 40 cycles. Dotted lines are used to label the possible fluoride compounds.

In comparison, Figure 9b shows strong Li-F peak before the etching treatment for the TiO_2-coated $LiCoO_2$ electrode, suggesting a much thinner organic layer formed on the TiO_2-coated $LiCoO_2$ electrode after the cycling test. Additionally, another peak at ~ 685.5 eV could be seen in the TiO_2-coated $LiCoO_2$ electrode, especially after a few steps of the etching treatment. This peak has been assigned to metal fluoride in other studies and could be assigned to Ti-F here because TiO_2 is a Lewis base that reacts with trace HF in electrolyte [40]. After 150 seconds of the etching treatment, the Li-F peak disappeared and left only the Ti-F peak, implying that Ti-F dominated the fluoride components on the surface of TiO_2-coated $LiCoO_2$ electrode. The formation of Ti-F consumed HF, which can be harmful to the cycling performance of battery electrolyte by leading to side reactions. Additionally, this metal fluoride layer is believed to have a higher chemical stability than the side products formed on the surface of the pristine $LiCoO_2$ [40]. This explained the phenomenon of less Co dissolution in the TiO_2-coated $LiCoO_2$ electrode after the cycling test, which led to much better high voltage cycling stability of the $LiCoO_2$ electrode after the TiO_2 coating.

Conclusions

This study explores the microwave radiation (MWR)-assisted synthesis as a surface engineering technique to grow TiO_2 and ZrO_2 coatings on the surface of LIB electrodes like $LiCoO_2$. This technique requires relatively short synthesis times and low synthesis temperature compared to traditional sol-gel and hydro/solvothermal synthesis methods. By selecting appropriate coating materials, like TiO_2, we altered the surface characteristics of $LiCoO_2$ and improved its electrochemical performance. The capacity remaining was improved from 52.8% to 81.9% and 84.4% after 40 cycles by the ZrO_2 and TiO_2 coating, respectively. These results suggest that further attention should be given to synthesis under electromagnetic fields, because they provide promising, alternative routes to engineer the surface of battery electrodes for improving their performance. Exploring the synthesis of other materials via this process, including both inorganic ceramics and organic polymers, will provide a novel pathway towards engineering advanced LIBs with high energy and power density, as well as extended lifespan.

Acknowledgments

This work was supported by National Science Foundation (NSF) CAREER Award (CMMI1751605) and INCUBATE seed funding from Carnegie Mellon University. Microwave field assisted TiO_2 synthesis efforts were supported by the DARPA AIRA Program (grant number HR00111990030). The authors acknowledge use of the Materials Characterization Facility at Carnegie Mellon University supported by grant MCF-677785. The Authors thank Dr. Joel Gillespie from the University of Pittsburgh Materials Characterization Laboratory for the access to the XPS spectrometer. Dr. Haiyan Wang and Ms. Xin Li Phuah acknowledge the support from the Office of Naval Research under Contract No. N00014-17-1-2087 and N00014-16-1-2778. This research used 6-ID-D beamline and other resources in Advanced Photon Source, Argonne National Laboratory under Contract No. DE-AC02-06CH11357.

Author contributions

Laisuo Su: Conceptualization, Experimental design, Carrying out Measurements, Manuscript composition. Shikhar Krishn Jha: Carrying out Measurements. Xin Li Phuah: Carrying out Measurements. Jiang Xu: Carrying out Measurements. Nathan Nakamura: Experimental design, Manuscript composition. Haiyan Wang: Resources, Funding acquisition. John S. Okasinski: Resources. B. Reeja-Jayan: Supervision, Experimental design, Resources, Manuscript composition, Funding acquisition.

Conflict of interest

All authors declare that they have no conflict of interest.

References:

[1] Kalluri, S.; Yoon, M.; Jo, M. et al. (2017), Surface engineering strategies of layered LiCoO2 cathode material to realize high-energy and high-voltage Li-ion cells., ADV ENERGY MATER 7:1601507.

[2] Su, L.; Smith, P. M.; Anand, P. et al. (2018), Surface engineering of a LiMn2O4 electrode using nanoscale polymer thin films via chemical vapor deposition polymerization., ACS APPL MATER INTER 10:27063-27073.
[3] Zhou, A.; Liu, Q.; Wang, Y. et al. (2017), Al2O3 surface coating on LiCoO2 through a facile and scalable wet-chemical method towards high-energy cathode materials withstanding high cutoff voltages., J MATER CHEM A 5:24361-24370.
[4] Dai, X.; Wang, L.; Xu, J. et al. (2014), Improved Electrochemical Performance of LiCoO2 Electrodes with ZnO Coating by Radio Frequency Magnetron Sputtering., ACS APPL MATER INTER 6:15853-15859.
[5] Dai, X.; Zhou, A.; Xu, J. et al. (2015), Superior electrochemical performance of LiCoO2 electrodes enabled by conductive Al2O3-doped ZnO coating via magnetron sputtering., J POWER SOURCES 298:114-122.
[6] Zhou, A.; Lu, Y.; Wang, Q. et al. (2017), Sputtering TiO2 on LiCoO2 composite electrodes as a simple and effective coating to enhance high-voltage cathode performance., J POWER SOURCES 346:24-30.
[7] Zhou, A.; Xu, J.; Dai, X. et al. (2016), Improved high-voltage and high-temperature electrochemical performances of LiCoO2 cathode by electrode sputter-coating with Li3PO4., J POWER SOURCES 322:10-16.
[8] Wang, L.; Chen, B.; Ma, J. et al. (2018), Reviving lithium cobalt oxide-based lithium secondary batteries-toward a higher energy density., CHEM SOC REV 47:6505-6602.
[9] Jha, S. K.; Phuah, X. L.; Luo, J. et al. (2018), The effects of external fields in ceramic sintering., J AM CERAM SOC
[10]Lidström, P.; Tierney, J.; Watheyb, B. et al. (2001), Microwave assisted organic synthesis - a review., TETRAHEDRON 57:9225-9283.
[11]Nakamura, N.; Terban, M. W.; Billinge, S. et al. (2017), Unlocking the Structure of Mixed Amorphous-Crystalline Ceramic Oxide Films Synthesized Under Low Temperature Electromagnetic Excitation., J MATER CHEM A
[12]Reeja-Jayan, B.; Harrison, K. L.; Yang, K. et al. (2012), Microwave-assisted Low-temperature Growth of Thin Films in Solution., SCI REP-UK 2:
[13]Bondioli, F.; Ferrari, A. M.; Leonelli, C. et al. (2001), Microwave‐hydrothermal synthesis of nanocrystalline zirconia powders., J AM CERAM SOC 84:2728-2730.
[14]Shah, J. J.; Mohanraj, K. (2014), Comparison of conventional and microwave-assisted synthesis of benzotriazole derivatives., INDIAN J PHARM SCI 76:46.
[15]Kim, K. C.; Jegal, J.; Bak, S. et al. (2014), Improved high-voltage performance of FePO4-coated LiCoO2 by microwave-assisted hydrothermal method., ELECTROCHEM COMMUN 43:113-116.
[16]Hoogenboom, R.; Schubert, U. S. (2007), Microwave-Assisted Polymer Synthesis: Recent Developments in a Rapidly Expanding Field of Research., MACROMOL RAPID COMM 28:368-386.
[17]Su, L.; Tong, P.; Zhang, L. et al. (2019), Photoelectrochemical immunoassay of aflatoxin B1 in foodstuff based on amorphous TiO2 and CsPbBr3 perovskite nanocrystals., The Analyst 144:4880-4886.
[18]Shu, J.; Qiu, Z.; Lv, S. et al. (2018), Plasmonic Enhancement Coupling with Defect-Engineered TiO2‐x: A Mode for Sensitive Photoelectrochemical Biosensing., ANAL CHEM 90:2425-2429.
[19]Kim, Y. J.; Cho, J.; Kim, T. et al. (2003), Suppression of Cobalt Dissolution from the LiCoO[sub 2] Cathodes with Various Metal-Oxide Coatings., J ELECTROCHEM SOC 150:A1723.
[20]Nakamura, N.; Seepaul, J.; Kadane, J. B. et al. (2017), Design for low‐temperature microwave‐assisted crystallization of ceramic thin films., APPL STOCH MODEL BUS 33:314-321.
[21]Jha, S. K.; Charalambous, H.; Okasinski, J. S. et al. (2019), Using in operando diffraction to relate lattice strain with degradation mechanism in a NMC battery., J MATER SCI 54:2358-2370.

[22]Jha, S. K.; Nakamura, N.; Zhang, S. et al. (2019), Defect‐Mediated Anisotropic Lattice Expansion in Ceramics as Evidence for Nonthermal Coupling between Electromagnetic Fields and Matter., ADV ENG MATER 1900762.
[23]Nakamura, N. J.; Culbertson, E.; Billinge, S. J. et al. (2019), The role of defects in microwave-assisted synthesis of cubic ZrO2.,
[24]Nam, K. M.; Shim, J. H.; Han, D. et al. (2010), Syntheses and Characterization of Wurtzite CoO, Rocksalt CoO, and Spinel Co3O4 Nanocrystals: Their Interconversion and Tuning of Phase and Morphology., CHEM MATER 22:4446-4454.
[25]Zhou, A.; Lu, Y.; Wang, Q. et al. (2017), Sputtering TiO2 on LiCoO2 composite electrodes as a simple and effective coating to enhance high-voltage cathode performance., J POWER SOURCES 346:24-30.
[26]Sun, Y.; Han, J.; Myung, S. et al. (2006), Significant improvement of high voltage cycling behavior AlF3-coated LiCoO2 cathode., ELECTROCHEM COMMUN 8:821-826.
[27]Schulz, N.; Hausbrand, R.; Wittich, C. et al. (2018), XPS-Surface Analysis of SEI Layers on Li-Ion Cathodes: Part II. SEI-Composition and Formation inside Composite Electrodes., J ELECTROCHEM SOC 165:A833-A846.
[28]Schulz, N.; Hausbrand, R.; Dimesso, L. et al. (2018), XPS-Surface Analysis of SEI Layers on Li-Ion Cathodes: Part I. Investigation of Initial Surface Chemistry., J ELECTROCHEM SOC 165:A819-A832.
[29]Yang, Z.; Li, R.; Deng, Z. (2018), A deep study of the protection of lithium cobalt oxide with polymer surface modification at 4.5 V high voltage., SCI REP-UK 8:
[30]Bai, Y.; Liu, N.; Liu, J. et al. (2006), Coating Material-Induced Acidic Electrolyte Improves LiCoO2 Performances., Electrochemical and Solid-State Letters 9:A552.
[31]Aurbach, D.; Markovsky, B.; Rodkin, A. et al. (2002), On the capacity fading of LiCoO2 intercalation electrodes:: the effect of cycling, storage, temperature, and surface film forming additives., ELECTROCHIM ACTA 47:4291-4306.
[32]Miyashiro, H.; Yamanaka, A.; Tabuchi, M. et al. (2006), Improvement of degradation at elevated temperature and at high state-of-charge storage by ZrO2 coating on LiCoO2., J ELECTROCHEM SOC 153:A348-A353.
[33]Cheng, H.; Wang, F.; Chu, J. P. et al. (2012), Enhanced cycleabity in lithium ion batteries: Resulting from atomic layer depostion of Al2O3 or TiO2 on LiCoO2 electrodes., The Journal of Physical Chemistry C 116:7629-7637.
[34]Jayasree, S. S.; Nair, S.; Santhanagopalan, D. (2018), Ultrathin TiO2 Coating on LiCoO2 for Improved Electrochemical Performance as Li-Ion Battery Cathode., CHEMISTRYSELECT 3:2763-2766.
[35]Hwang, B. J.; Chen, C. Y.; Cheng, M. Y. et al. (2010), Mechanism study of enhanced electrochemical performance of ZrO2-coated LiCoO2 in high voltage region., J POWER SOURCES 195:4255-4265.
[36]Chung, K. Y.; Yoon, W.; Lee, H. S. et al. (2006), In situ XRD studies of the structural changes of ZrO2-coated LiCoO2 during cycling and their effects on capacity retention in lithium batteries., J POWER SOURCES 163:185-190.
[37]Yu, J.; Han, Z.; Hu, X. et al. (2014), The investigation of Ti-modified LiCoO2 materials for lithium ion battery., J POWER SOURCES 262:136-139.
[38]Zhang, J.; Wang, R.; Yang, X. et al. (2012), Direct Observation of Inhomogeneous Solid Electrolyte Interphase on MnO Anode with Atomic Force Microscopy and Spectroscopy., NANO LETT 12:2153-2157.
[39]Kerlau, M.; Kostecki, R. (2006), Interfacial Impedance Study of Li-Ion Composite Cathodes during Aging at Elevated Temperatures., J ELECTROCHEM SOC 153:A1644.
[40]Zhou, A.; Lu, Y.; Wang, Q. et al. (2017), Sputtering TiO2 on LiCoO2 composite electrodes as a simple and effective coating to enhance high-voltage cathode performance., J POWER SOURCES 346:24-30.